RSC Advances

ROYAL SOCIETY OF CHEMISTRY

www.rsc.org/advances

Modelling the interaction of graphene oxide using an atomistic-continuum model

TOM DYER[1], NGAMTA THAMWATTANA[1], and ROUHOLLAH JALILI[2]

[1]*School of Mathematics and Applied Statistics, University of Wollongong, Wollongong, NSW 2522, Australia*
[2]*ARC Centre of Excellence for Electromaterials Science, Intelligent Polymer Research Institute, AIIM Facility, Innovation Campus, University of Wollongong, Wollongong, New South Wales, 2522, Australia*

Abstract

In this paper, we construct a continuum model for graphene oxide based upon the Lerf-Klinowski structure to investigate the interaction forces between sheets of graphene oxide. We use the Lennard-Jones potential and Coloumbic potential to determine the total potential energy between sheets of graphene oxide. We analytically calculate the interaction forces within the system using sums of hypergeometic functions. Our model is then modified to investigate different levels of hydration and oxidation within the system. Our investigations are reconstructed using the LAMMPS molecular dynamics simulator and we find that the analytical solution quickly and effectively calculates results that match well against our simulation data and values given from literature.

I. INTRODUCTION

Graphene science is a rapidly growing field with a plethora of potential applications including composites, energy storage and conversion, nanoelectronics, transparent conducting films and multifunctional 3D structures [1, 2, 3, 4, 5, 6] . The chemical exfoliation of graphite is the most practical method for production of graphene. In this method, a graphene dispersion is obtained through the oxidation of natural or synthetic graphite to give graphite oxide that can be exfoliated in water or organic solvents to generate single sheets of graphene oxide (GO) [7, 8, 9, 10]. This dispersed GO can then be utilised to fabricate devices directly or via composite formation, followed by reduction to graphene [11, 12]. In this regard, understanding of the GO sheets interactions offers a significant advantage to extent our ability to readily process and fabricate them into a wide variety of structures using a number of different 3D fabrication techniques [13]. The oxidation process causes the disruption of sp^2 networks in the structure of GO. As a result of this, GO has little thermal or electronic conductive properties [10]. However, GO is hydrophillic and can be easily dispersed in water and many organic solvents. This high solubility suggests a use in medical applications, notably in drug delivery [14].

When graphene is oxidised to form GO, various functional groups and deformations are introduced to the graphene basal plane. Some of the bonds between carbon atoms are stretched and distorted by the presence of the functional groups which displace the attached carbon atoms slightly out of the plane forming a sp^3 hybrid carbon structure [15]. Graphene oxide (GO) consists of a basal plane of sp^2 carbon with oxidated functional groups decorating both sides of the structure [10]. The exact chemical structure of GO has long been the subject of debate and no definitive model exists [10]. Originally, GO models were constructed as a periodic, regular lattice structure. The

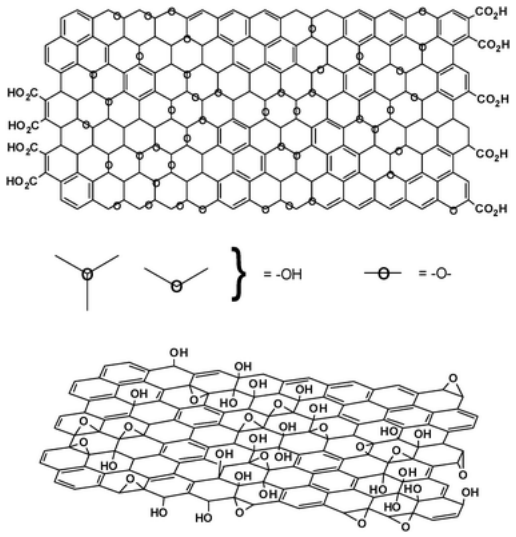

Figure 1: *The Lerf-Klinowski Model [10]*

Hofmann model consists of epoxy groups spread over the basal plane with a general formula of C_2O. This model was later modified by Ruess who included hydroxyl groups into the structure to account for the hydrogen content of GO and well as modifying the hybridisation of the basal structure to a sp^3 system. The Scholz-Boehm model removed the epoxide groups.

In 1998, Lerf et al constructed a model, as shown in Figure 1, where the main functional groups attached to the basal plane consist of epoxy (C-O-C) and hydroxyl (C-OH) groups with carboxyl and carbonyl groups attached to the edges of the carbon structure [16, 17]. Unlike earlier structures, the Lerf-Klinowski model is non-periodic. This model of GO is nonstoichiometric and predominantly amorphous due to distortions from the high fraction of sp^3 C-O bonds [15]. The Lerf-Klinowski model has become the most widely accepted model for GO in recent times and further nuclear magnetic resonance (NMR) experimental results support the model [10, 18, 19]. In constructing the model, Lerf et al have performed several investigations on the hydration properties of GO. This paper aims to replicate these experimental results using analytical techniques.

In this paper, we investigate the interaction forces between sheets of GO. We adopt the Lerf-Klinowski structural model to construct a surface representation of GO using a series of continuous and flat disk surfaces. The interaction energy (E) is defined as the total energy induced between our molecules by van der Waals and electrostatic forces. All other forces are considered trivial. Van der Waals force is calculated using the Lennard-Jones potential function and electrostatic force using the Coulomb potential. We successfully analytically calculate the interaction forces within the system using sums of hypergeometric functions. These equation are then applied to sheets of GO under different conditions of both oxidation and hydration. The composition of the GO sheets is varied so we are able to view the change in the energy given different levels of oxidation. We also simulate hydration by inserting monolayers of water between sheets of GO. We find that the analytical solution quickly and effectively calculates results that match well against molecular dynamic simulation data and values given from literature.

II. Modelling approach

Using the continuum approach for modelling nanostructures as demonstrated by Cox et al [20], we construct our model of GO from a series of continuous sheets. Firstly, we detail the structure of the functional groups used to construct the model, then we determine the interaction energy between two sheets of the GO model based on the van der Waals force, represented by the the 6-12 Lennard Jones potential, and the electrostatic potential, represented using the Coloumbic point-charge.

I. Structure of functional groups

We use the Lerf-Klinowski model to represent our GO structure. As discussed earlier, the hexagonal lattice of carbon atoms comprising the base of the GO structure is distorted but still largely intact. Consequently, we ignore these distortions in our model of GO and assume the carbon atoms are structured like an unaffected graphene sheet.

The energies of a GO sheet are greatly reduced when epoxy and hydroxyl groups are gathered together in one area [21]. However despite this, the arrangement of the functional groups on the GO sheet still largely depends on the method and conditions involved during synthesis [18]. We follow studies by Mkhoyan et al which suggest the functional groups form a uniformly random distribution on both sides of the sheet [15].

We use the structure of the epoxy and hydroxyl groups from the DFT study performed by Yan et al [21] to derive the positions of the oxygen and hydrogen atoms relative to the carbon plane. An epoxy functional group is constructed of a single oxygen atom bonded to two neighbouring carbon atoms. The C–O bond length at relaxation is given to be 1.44 Å and the two attached carbons C–C bond length is stretched to 1.51 Å . Further distortions include the carbon atoms moving out of the plane by 0.34 Å . From this information, we deduce that the oxygen atoms lie at a perpendicular distance of $(1.23 + 0.34)/2 = 1.57$ Å from the carbon basal plane. A hydroxyl functional group is constructed of a OH group bonded to a carbon atom. The C–O bond length at relaxation is given to be 1.44 Å , the O–H bond length is given as 0.98 Å and the C–O–H bond angle is 107.9°. The attached carbon atom is distorted out of the plane by 0.37 Å . For simplicity, we assume the hydrogen and oxygen atoms lie in the same plane perpendicular to the basal plane. Then, we find the hydrogen and oxygen atoms lie at perpendicular distance of $1.37 + 0.37 = 1.74$ Å from the basal plane. Taking the average of the C–O distance in hydroxyl and the height of the epoxy group, we get a value of $(1.57 + 1.74)/2 = 1.66$ Å for the averaged height of an oxygen/hydrogen atom from the basal plane.

II. Continuum approach

We represent a single sheet of GO using a construction of three distinct, continuous, flat surfaces, each lying perpendicular to the same axis. The central surface represents a sheet of graphene, while the upper and lower surfaces represent the attached functional groups as illustrated in Figure 2. The basal plane of carbon is assumed to be fundamentally identical to sp^2 graphene. The surfaces representing the functional groups are modelled as two surfaces of combined oxygen/hydrogen, representing the attached epoxy (C–O–C) and hydroxyl (C– OH) elements, positioned both above and below the carbon sheet and separated by a distance of 1.66 Å . We assume that in this continuous approximation, the atoms are distributed uniformly on each surface.

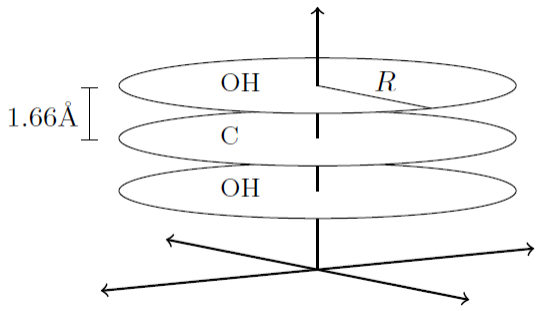

Figure 2: *A continuum model for a single GO sheet represented by a surface of graphene and two surfaces of mixed hydrogen and oxygen atoms.*

The continuum approach of modelling discrete atomic structure as continuous surfaces has been used previously for calculating various van der Waals interaction between carbon nanostructures [20]. We aim to use this model to reduce the computation costs involved with the modelling interactions of GO structures that would be necessary when using a molecular dynamics (MD) simulation or any other discrete approach. We determine the interaction energy between two atoms on distinct molecules using the Lennard-Jones potential function which incorporates both the van der Waals attraction force and Pauli repulsion force between the molecules. The 6-12 Lennard-Jones potential function is written in the form, $\phi(\rho) = -A/\rho^6 + B/\rho^{12}$, where ρ is the distance between the two atoms and A and B are the appropriate attractive and repulsive Lennard-Jones constants. The presence of the oxygenated groups introduces a charged potential between the two sheets so electrostatic forces must also be considered. This electrostatic potential between two discrete, charged atoms is calculated using the Coulomb potential which is defined as, $q_1 q_2 / 4\pi\epsilon_0\rho$, where q_1, q_2 are the partial atomic charges on each atom, ϵ_0 is the permittivity constant and ρ is the distance between the two atoms.

The total non-bonded interaction energy (E) is determined by summing all of the interactions between every pair of atoms. That is,

$$E = \sum_i \sum_j \left[\phi(\rho_{ij}) + \frac{q_i q_j}{4\pi\epsilon_0 \rho_{ij}} \right],$$

where i, j iterate over all the atoms on each molecule respectively, q_i and q_j are the charges of the i-th and j-th atoms respectively and ρ_{ij} is the distance between the i-th and j-th atoms. However these calculations become quite computationally costly when dealing with large numbers of atoms. Using continuum methods as in [20], our atoms are assumed to be evenly distributed over the surface. Thus, we calculate the energy between any two surfaces as,

$$E = \eta_1 \eta_2 \iint_{S_1} \iint_{S_2} \left[\phi(\rho) + \frac{q_{S_1} q_{S_2}}{4\pi\epsilon_0 \rho} \right] dS_1 dS_2, \tag{1}$$

where η_1 and η_2 are the uniform surface density of the atoms on the surfaces S_1 and S_2 respectively, where q_{S_1} and q_{S_2} are the average charges of the surfaces S_1 and S_2 respectively and ρ is the distance between the two surfaces.

The total interaction energy between two sheets of GO is the sum of all surface interactions. These interactions consist of the interaction between the two graphene surfaces (E_{G-G}), the total

interaction between a graphene surface and the oxygen/hydrogen surface on different GO sheets (E_{G-OH}) and the total interactions between each pair of oxygen/hydrogen surface on different GO sheets (E_{OH-OH}). We define $E = E(z)$ so we calculate the variation in interaction energy as the distance between the two sheets varies along the z-axis as shown in Figure 3. Summing all our interactions gives us

$$E(z) = E_{G-G}(z) + 2E_{G-OH}(z+\delta) + 2E_{G-OH}(z-\delta) + 2E_{OH-OH}(z) + E_{OH-OH}(z+2\delta) + E_{OH-OH}(z-2\delta),$$

where z is the distance between the carbon planes on the two GO sheets and δ is the distance between the carbon plane and the oxygen/hydrogen planes.

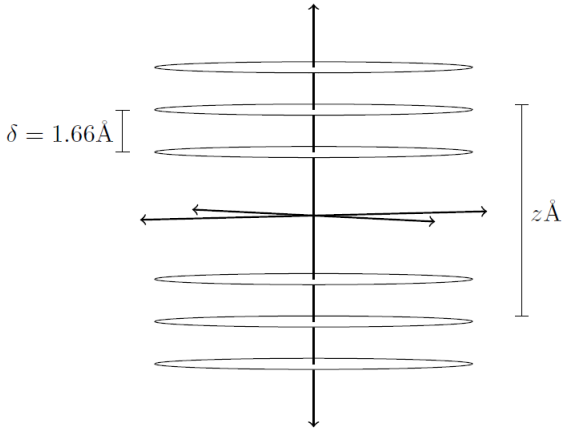

Figure 3: *Interaction between two GO sheets. Here, z is the distance between the sheets and δ is the distance between the C and OH layers.*

The various constants used in our model are now defined. Firstly, the Lennard-Jones constants are taken from the Universal Force Field (UFF) atomic potentials [22] and are shown in Table 1. In the cases where we must determine the Lennard Jones constants for a pair of different atoms, we use the Lorentz-Berthelot mixing rules defined as $\epsilon_{xy} = (\epsilon_x \epsilon_y)^{1/2}$ and $\sigma_{xy} = (\sigma_x + \sigma_y)/2$.

Table 1: *Lennard-Jones constants.*

	C	O	H
ϵ (eV)	0.0045	0.0026	0.0019
σ (Å)	3.851	3.500	2.886
A (eV Å^{-6})	29.45	9.49	2.19
B (eV Å^{-12})	48033.03	8718.39	631.65

The point charges required to measure the Coloumbic potential is taken from the atomic point charge model calcualted by Stauffer et al for the electrostatic potential (ESP) of GO from *ab initio* calculations [23]. We use the simple ESP charges defined in [23] shown in Table 2, which also includes the ESP of water necessary for later use in Section IV. We use the permittivity constant for water $\epsilon_0 = 1.3245 \times 10^{-7}$ F/m.

Table 2: *Electrostatic potential of charged groups on graphene oxide.*

	Atom	ESP
Water	O	$-0.56e$
	H	$+0.28e$
Epoxy	O	$-0.24e$
	C	$+0.12e$
Hydroxyl	O	$-0.38e$
	C	$+0.12e$
	H	$+0.26e$

The density of our carbon graphene surface is taken to be $\eta = 0.3812\,\text{Å}^{-2}$ [20]. We then take the density of the oxygen/hydrogen surfaces from the C/O ratio of the GO sheet which vary given the oxidation of the sheet. Note that the comparative density of the oxygen and hydrogen atoms must be halved as they are distributed over two surfaces.

Recall from equation (1) that the interaction energy between two surfaces S_1 and S_2 is expressed as

$$E = \eta_1\eta_2 \iint_{S_1}\iint_{S_2} \left[\phi(\rho) + \frac{q_{S_1}q_{S_2}}{4\pi\epsilon_0\rho}\right] dS_1 dS_2.$$

This surface integral is now applied to the circular sheets of the GO model using polar coordinates.

$$E = \eta_1\eta_2 \int_0^{2\pi}\int_0^{R}\int_0^{R}\int_0^{2\pi} \left(\phi(\rho) + \frac{q_{S_1}q_{S_2}}{4\pi\epsilon_0\rho}\right) r_1 r_2\, d\theta_1 dr_1 dr_2 d\theta_2. \tag{2}$$

An arbitrary point on each circular surface is represented in polar coordinates as $(r_2\cos\theta_2, r_2\sin\theta_2, Z)$ and $(r_1\cos\theta_1, r_1\sin\theta_1, 0)$. The distance between two arbitrary points is simply $\rho^2 = (r_2\cos\theta_2 - r_1\cos\theta_1)^2 + (r_2\sin\theta_2 - r_1\sin\theta_1)^2 + Z^2$. Due to the angular symmetry of the circular sheets, we fix $\theta_2 = 0$. Then, taking $\theta = \theta_1$ to simplify our notation, we have

$$\begin{aligned}\rho^2 &= (r_2 - r_1\cos\theta)^2 + r_1^2\sin^2\theta + Z^2 \\ &= r_1^2 + r_2^2 - 2r_1r_2\cos\theta + Z^2.\end{aligned}$$

As θ_2 is fixed to be constant, equation (2) becomes

$$E = 2\pi\eta_1\eta_2 \int_0^{R_1}\int_0^{R_2}\int_{-\pi}^{\pi} r_1 r_2 \left(-\frac{A}{\rho^6} + \frac{B}{\rho^{12}} + \frac{q_{S_1}q_{S_2}}{4\pi\epsilon_0\rho}\right) d\theta dr_1 dr_2.$$

We simplify this integral by using hypergeometric functions, the details of which are explained in Appendix A. The final result for the interaction energy is

$$E = 2\pi\eta_1\eta_2 \left(-AJ(3) + BJ(6) + \frac{q_{S_1}q_{S_2}}{4\pi\epsilon_0} J(1/2)\right)$$

where

$$J(n) = \sum_{m=0}^{\infty} \frac{(\frac{n}{2})_m (\frac{n+1}{2})_m}{(m!)^2} \frac{4^m (R_1 R_2)^{2m+2}}{(2m+2)^2} \sum_{q=0}^{\infty} \frac{(2m+n)_q}{(m+2)_q} \frac{R_1^{2q}}{(R_1^2+R_2^2+z^2)^{q+2m+n}} F\left(q+2m+n, 1; m+2; \frac{R_2^2}{R_1^2+R_2^2+z^2}\right).$$

Here $F(a,b;c;z)$ defines a ordinary hypergeometric function and $(x)_n$ represents the rising pochhammer symbol.

III. Effects of various oxidation levels on the interlayer distance between GO sheets

GO is a loosely defined material which can have varying structure and properties depending on the level of oxidation. Partial oxidation is considered to be thermodynamically favourable and chemically reduced forms of GO are often considered more useful in many applications [10]. The degree of oxidation of GO varies depending on the synthesis conditions.The typical measure of the oxidation level is the ratio of carbon and oxygen atoms [24]. Generally, the range of oxidation varies from a C:O ratio of 4:1 to 2:1, although chemical reduction give a ratio of 12:1 and higher [25, 24]. Fully oxidised graphene oxide has around 50 percent coverage of functional groups and an ideal composition of $C_8O_2(OH)_2$ or $C_6O_1(OH)_2$ [24].

Different degrees of oxidation are simulated with the above GO model by varying the density of the oxygen/hydrogen layers. Here we show the interaction energy for three differently oxidised GO sheets.

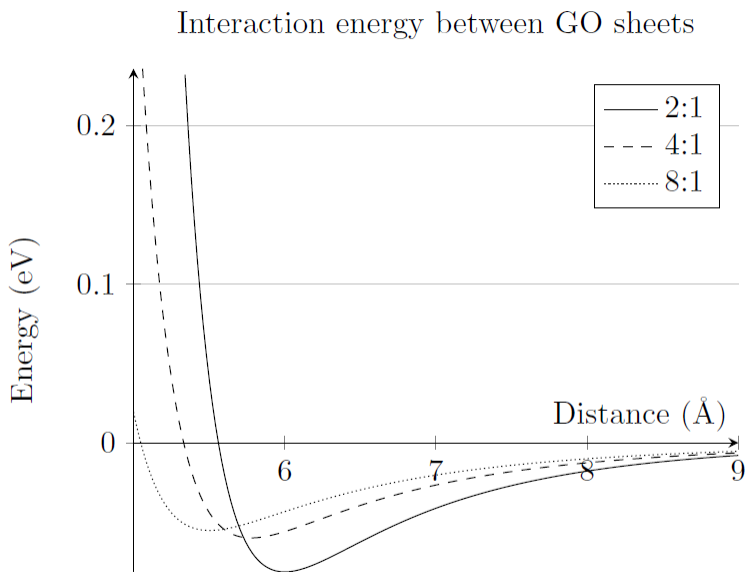

Figure 4: *The interaction energy between two graphene oxide sheets, shown at a C:O ratio of 2:1, 4:1 and 8:1.*

We see that the functional groups are indeed instrumental for determining the interlayer distance and energy between GO sheets where the interlayer distance is the distance at which the interaction

energy between the two layers is minimised. We also see clearly that the more oxidised a sheet of graphene oxide, the further apart the interlayer distance and the stronger the binding energy between two sheets. This interlayer distance matches well with that of dehydrated graphene oxide which have been experimentally measured at values from 5.9 to 6.7 Å [26, 27].

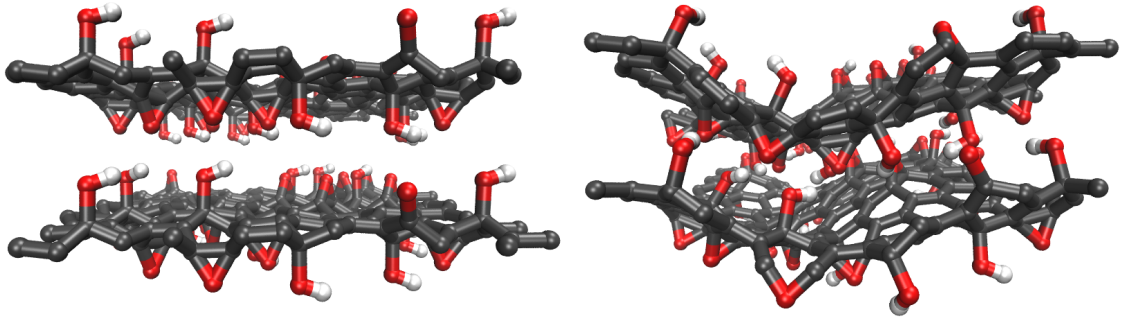

a b

Figure 5: *a) A pair of 2nm × 2nm periodic sheets of GO shown after minimisation. b) The same sheets displayed after a 1000ps simulation. Both images are created using the Visual Molecular Dynamics (VMD) molecular visualization program [28].*

As a comparison to the analytical result, a molecular dynamics simulation was run, the setup conditions of which are explained in Appendix C. A pair of periodic GO sheets were constructed and the system was then run until equilibrium was reached. After the simulation is completed, as shown in Figure 5, the averaged interlayer distance between the sheets was found as 4.7 Å . This is reasonably comparable to the value of 5.7 Å given by the equivalent analytical result. It is likely the difference between the results is largely caused by the distribution of the functional groups on the surface.

IV. Effects of hydration on the interlayer distance between GO sheets

GO is highly absorbent and tends to have some water molecules collected between the layers. We examine the effect of this intercalated water on the intermolecular distance by inserting a monolayer of water between the two GO sheets.

The oxygenated functional groups on the surface of GO cause it to have strongly hydrophillic properties [25]. Subsequently, it is very hard to remove all the water from GO and intermellar water molecules are always present in the structure, even after prolonged drying [29, 30]. Intercalated water has only marginal effects on the layer structure of GO sheets, however it causes the interlayer distance to increase to as high as 12 Å [10, 24].

The hydrogen atoms in the water couple to the oxygens in the functional groups via hydrogen bonds or electrostatic interactions [31]. The electrostatic interactions between the oxygenated groups and water form an interfacial H-bond network, that is, the interaction between the layers is mediated by a network of hydrogen bonded water molecules [32]. As GO becomes more hydrated, there is a gradual, linear increase in the interlayer distance. However, once the hydration of the GO sheets passes around 75 percent humidity, the interlayer distance between the sheets sharply increases in steplike transitions. This suggests the introduction of monolayers of water between the sheets [27, 31, 33].

We represent the intercalated water as a surface fixed directly in the centre of the two GO layers. The GO sheets are then allowed to interact as before, with the inclusion of additional interactions between each GO surface and the water surface.

$$E = E_{GO} + 2 \cdot (E_{G-W} + E_{OH-W}).$$

We use the same values for the oxygen and hydrogen Lennard-Jones constants as we did for our GO sheet. We represent our water as a point on a flat surface. We approximate the area occupied by a molecule of water as the area of a circle with radius equal to the molecular distance of water at room temperature or 2.965 Å [34]. The density of water molecules on this surface is then equal to $1/(\pi \cdot 2.965^2) = 0.0362077$ Å $^{-2}$. Consequently, the density of hydrogen is 0.024138 Å $^{-2}$ and the density of oxygen is 0.012069 Å $^{-2}$.

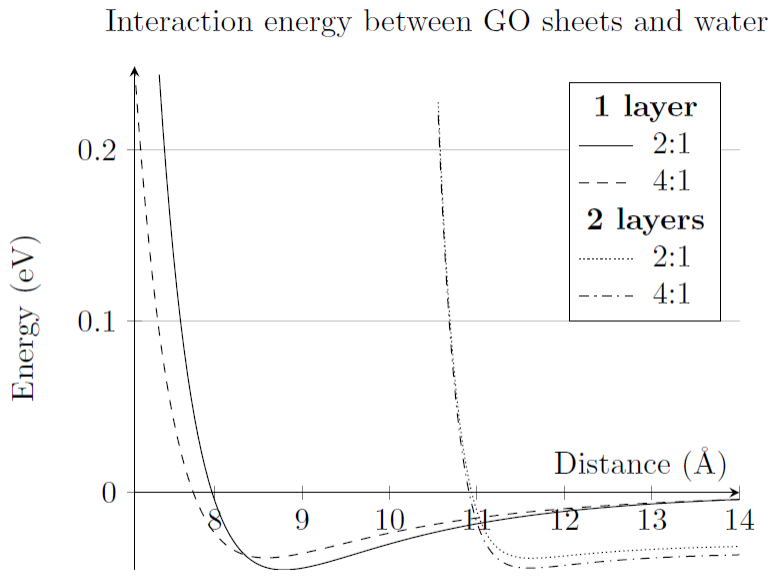

Figure 6: *The interaction energy between two graphene oxide sheets with layers of water intercalated between the sheets.*

We observe upon adding each successive layer of water between the sheets, the interlayer distance increases by around 3 Å. This corrolates with experimental results which suggest the insertion of a water monolayer causes a jump of an equivalent degree in the interlayer distance [27, 33]. Fully hydrated GO has sample values measured up to 12 Å in [27] which is similar to the result given by adding two monolayers of water to the model. After two layers of water has been intercalated between the pair of sheets, the properties of any additional water is indistiguishable from bulk water, i.e. the GO sheets are not simply hydrated but are considered to be fully separated [31].

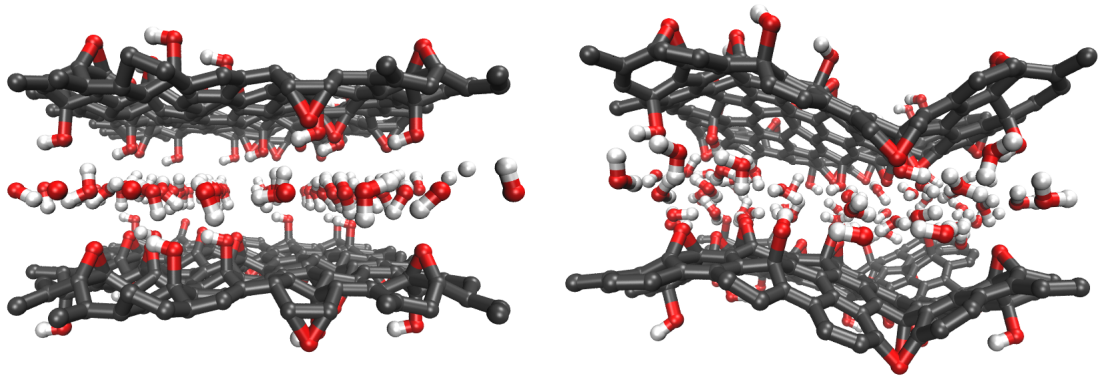

a b

Figure 7: *a) A pair of 2nm × 2nm periodic sheets of GO separated with water molecules shown after minimisation. b) The same sheets displayed after a 1000ps simulation.*

A molecular dynamics simulation of GO was repeated, now with a single layer of water molecules distributed between the sheets. The interlayer distance between the sheets after equilibrium is given as 7.7 Å after the simulation is completed as seen in Figure 7.

III. Conclusions

This paper considered an analytical model for calculating interaction energy between sheets of graphene oxide. Our model is then modified to investigate different levels of hydration and oxidation within the system. Our investigations are reconstructed using the LAMMPS molecular dynamics simulator and we find that the analytical solution quickly and effectively calculates results that match well against our simulation data and values given from literature. The techniques used to derive the energy are able to be used for any disk-disk type molecular interaction. Knowledge of the interlayer distance between sheets of graphene oxide with different hydration and oxidation levels would be useful for tailoring the materials for applications such as a carrier for drug-delivery and energy storage.

IV. Acknowledgements

Funding from the Australian Research Council Centre of Excellence Scheme (Project Number CE 140100012) is gratefully acknowledged by RJ.

A. Interaction energy between two disks

We have our interaction energy between two disks as

$$\begin{aligned} E &= 2\pi\eta_1\eta_2 \int_0^{R_1}\int_0^{R_2}\int_{-\pi}^{\pi} r_1 r_2 \left(-\frac{A}{\rho^6} + \frac{B}{\rho^{12}} + \frac{q_{S_1}q_{S_2}}{4\pi\epsilon_0\rho}\right) d\theta dr_1 dr_2 \\ &= 2\pi\eta_1\eta_2 \left(-AJ(3) + BJ(6) + \frac{q_{S_1}q_{S_2}}{4\pi\epsilon_0} J(1/2)\right), \end{aligned} \tag{3}$$

where

$$J(n) = \int_0^{R_1}\int_0^{R_2}\int_{-\pi}^{\pi} \frac{r_1 r_2}{\rho^{2n}}\, d\theta\, dr_1\, dr_2.$$

In order to solve this, we start by taking the integral

$$J_1(n) = \int_{-\pi}^{\pi} \frac{1}{\rho^{2n}}\, d\theta.$$

As $\cos\theta$ is an even function, we have

$$J_1(n) = 2\int_0^{\pi} \frac{1}{(r_1^2 + r_2^2 + z^2 - 2r_1 r_2\cos\theta)^n}\, d\theta.$$

Let $K_1 = r_1^2 + r_2^2 + z^2$ and $K_2 = 2r_1 r_2$. Then

$$J_1(n) = 2\int_0^{\pi} \frac{1}{(K_1 - K_2\cos\theta)^n}\, d\theta.$$

Using the identity $\cos\theta = 1 - 2\sin^2(\theta/2)$, we get

$$\begin{aligned} J_1(n) &= 2\int_0^{\pi} \frac{1}{(K_1 + K_2 - 2K_1\sin^2(\theta/2))^n}\, d\theta \\ &= \frac{2}{(K_1+K_2)^n}\int_0^{\pi} \frac{1}{(1 - \frac{2K_1}{K_1+K_2}\sin^2(\theta/2)))^n}\, d\theta. \end{aligned}$$

We simplify our function by taking $\omega = \theta/2$. Now

$$J_1(n) = \frac{4}{(K_1+K_2)^n}\int_0^{\pi/2} \frac{1}{(1 - \frac{2K_1}{K_1+K_2}\sin^2\omega)^n}\, d\omega.$$

We convert this integral into the form of a hypergeometric function by taking $t = \sin^2\theta$ and $d\theta = \frac{1}{2}t^{1/2}(1-t)^{-1/2}\, dt$.

$$\begin{aligned} J_1(n) &= \frac{2}{(K_1+K_2)^n}\int_0^{\pi/2} t^{1/2}(1-t)^{-1/2}\left(1 - \frac{2K_1}{K_1+K_2}t\right)^{-n} dt \\ &= \frac{2\pi}{(K_1+K_2)^n} F\left(n, \frac{1}{2}; 1; \frac{2K_1}{K_1+K_2}\right). \end{aligned}$$

We use the quadratic transformation $F(a,b;2b;z) = (1-\frac{z}{2})^{-a}F\left(\frac{a}{2}, \frac{a+1}{2}, b+\frac{1}{2}, \left(\frac{z}{2-z}\right)^2\right)$ to convert our function into the more convenient form

$$J_1(n) = \frac{2\pi}{K_1^n} F\left(\frac{n}{2}, \frac{n+1}{2}; 1; \left(\frac{K_2}{K_1}\right)^2\right).$$

We take

$$\begin{aligned}
J_2(n) &= \int_0^{R_1} r_1 \cdot J_1(n)\, dr_1 \\
&= \int_0^{R_1} \frac{r_1}{(r_1^2+r_2^2+z^2)^n} F\left(\frac{n}{2}, \frac{n+1}{2}, 1, \left(\frac{2r_1r_2}{r_1^2+r_2^2+z^2}\right)^2\right) dr_1 \\
&= \int_0^{R_1} \frac{r_1}{(r_1^2+r_2^2+z^2)^n} \sum_{m=0}^{\infty} \frac{(\frac{n}{2})_m (\frac{n+1}{2})_m}{(m!)^2} \left(\frac{2r_1r_2}{r_1^2+r_2^2+z^2}\right)^{2m} dr_1 \\
&= \sum_{m=0}^{\infty} \frac{(\frac{n}{2})_m (\frac{n+1}{2})_m}{(m!)^2} (2r_2)^{2m} \int_0^{R_1} \frac{r_1^{2m+1}}{(r_1^2+r_2^2+z^2)^{2m+n}}\, dr_1.
\end{aligned}$$

Taking $\alpha = r_2^2 + z^2$ to simplify our working, we get

$$J_2(n) = \sum_{m=0}^{\infty} \frac{(\frac{n}{2})_m (\frac{n+1}{2})_m}{(m!)^2} (2r_2)^{2m} \int_0^{R_1} \frac{r_1^{2m+1}}{(r_1^2+\alpha)^{2m+n}}\, dr_1.$$

We solve this integral using the method in Appendix B to get

$$J_2(n) = \sum_{m=0}^{\infty} \frac{(\frac{n}{2})_m (\frac{n+1}{2})_m}{(m!)^2} \frac{(2r_2)^{2m} R_1^{2m+2}}{(2m+2)(R_1^2+\alpha)^{2m+n}} F\left(2m+n, 1; m+2; \frac{R_1^2}{R_1^2+\alpha}\right).$$

Finally, we must solve

$$\begin{aligned}
J(n) &= \int_0^{R_2} r_2 \cdot J_2(n)\, dr_2 \\
&= \sum_{m=0}^{\infty} \frac{(\frac{n}{2})_m (\frac{n+1}{2})_m}{(m!)^2} \frac{4^m R_1^{2m+2}}{(2m+2)} \int_0^{R_2} \frac{r_2^{2m+1}}{(R_1^2+\alpha)^{2m+n}} \cdot F\left(2m+n, 1; m+2; \frac{R_1^2}{R_1^2+\alpha}\right) dr_2 \\
&= \sum_{m=0}^{\infty} \frac{(\frac{n}{2})_m (\frac{n+1}{2})_m}{(m!)^2} \frac{4^m R_1^{2m+2}}{(2m+2)} \sum_{q=0}^{\infty} \frac{(2m+n)_q (1)_m}{(m+2)_q q!} \int_0^{R_2} \frac{r_2^{2m+1}}{(R_1^2+\alpha)^{2m+n}} \cdot \left(\frac{R_1^2}{R_1^2+\alpha}\right)^q dr_2 \\
&= \sum_{m=0}^{\infty} \frac{(\frac{n}{2})_m (\frac{n+1}{2})_m}{(m!)^2} \frac{4^m R_1^{2m+2}}{(2m+2)} \sum_{q=0}^{\infty} \frac{(2m+n)_q}{(m+2)_q} R_1^{2q} \int_0^{R_2} \frac{r_2^{2m+1}}{(r_2^2+R_1^2+z^2)^{q+2m+n}}\, dr_2.
\end{aligned}$$

We solve this integral using the method in Appendix B to get

$$\begin{aligned}
J(n) = &\sum_{m=0}^{\infty} \frac{(\frac{n}{2})_m (\frac{n+1}{2})_m}{(m!)^2} \frac{4^m (R_1R_2)^{2m+2}}{(2m+2)^2} \\
&\sum_{q=0}^{\infty} \frac{(2m+n)_q}{(m+2)_q} \frac{R_1^{2q}}{(R_1^2+R_2^2+z^2)^{q+2m+n}} F\left(q+2m+n, 1; m+2; \frac{R_2^2}{R_1^2+R_2^2+z^2}\right),
\end{aligned}$$

which can be substituted into equation (3) to get our interaction energy between two disks as required.

B. Integration method required for deriving interaction energy

We want to solve an integral with the form

$$\begin{aligned} S(n) &= \int_0^R \frac{x^m}{(x^2+\alpha)^n}\,dx \\ &= \alpha^{-m}\int_0^R \frac{x^m}{(1+\frac{x^2}{\alpha})^n}\,dx. \end{aligned}$$

Let $t = \frac{x^2}{\alpha}$, then $x = (\alpha t)^{1/2}$ and $dx = \frac{1}{2}\alpha(\alpha t)^{-1/2}\,dt$. Our equation becomes

$$\begin{aligned} S(n) &= \frac{1}{2}\alpha^{1-n}\int_0^{R^2/\alpha}(1+t)^{-n}(\alpha t)^{m/2}(\alpha t)^{-1/2}\,dt \\ &= \frac{1}{2}\alpha^{(m-2n+1)/2}\int_0^{R^2/\alpha}(1+t)^{-n}t^{(m-1)/2}\,dt. \end{aligned}$$

Let $t' = \frac{\alpha t}{R^2}$, $dt' = \frac{\alpha}{R^2}\,dt$ to force our limits to the interval $[0,1]$. We get

$$\begin{aligned} S(n) &= \frac{1}{2}\alpha^{(m-2n+1)/2}\int_0^1 \left(1+\frac{R^2}{\alpha}t'\right)^{-n}\left(\frac{R^2}{\alpha}t'\right)^{(m-1)/2}\frac{R^2}{\alpha}\,dt' \\ &= \frac{1}{2}\alpha^{-n}R^{m+1}\int_0^1 \left(1+\frac{R^2}{\alpha}t'\right)^{-n}t'^{(m-1)/2}\,dt'. \end{aligned}$$

Let $t' = 1-s$, $dt' = -ds$ to convert our integral into a form that is easier to work with.

$$\begin{aligned} S(n) &= \frac{1}{2}\alpha^{-n}R^{m+1}\int_1^0 -\left(1+\frac{R^2}{\alpha}(1-s)\right)^{-n}(1-s)^{(m-1)/2}\,ds \\ &= \frac{1}{2}\alpha^{-n}R^{m+1}\left(\frac{R^2+\alpha}{\alpha}\right)^{-n}\int_0^1 \left(1-\frac{R^2}{R^2+\alpha}s\right)^{-n}(1-s)^{(m-1)/2}\,ds \\ &= \frac{1}{2}R^{m+1}(R^2+\alpha)^{-n}\int_0^1 \left(1-\frac{R^2}{R^2+\alpha}s\right)^{-n}(1-s)^{(m-1)/2}\,ds. \end{aligned}$$

We now write our integral in the form of a hypergeometric function

$$S(n) = \frac{R^{m+1}}{(m+1)(R^2+\alpha)^n}F\left(n,1;\frac{m+3}{2},\frac{R^2}{R^2+\alpha}\right).$$

C. Molecular dynamics simulation setup

Molecular dynamics (MD) simulations were performed using the Large-scale Atomic/Molecular Massively Parallel Simulator (LAMMPS) MD simulator. A pair of graphene oxide sheets were modelled in a 2nm $\times$ 2nm simulation box. This system was repeated periodically to represent an infinite sheet of graphene oxide and water molecules were inserted between the two sheets. The number of epoxy and hydroxyl groups was kept the same and were distributed randomly over both sides of each sheet to give a C:O ratio of 1:4. The water was simulated using the extended simple point charge (SPC/E) water model. The SHAKE algorithm was applied to the water to reduce high frequency vibrations of the hydrogen bonding. The interactions between the graphene

oxide molecules were modelled using the reactive forcefield ReaxFF which is known to be accurate in modelling hydrocarbon nanostructures [35]. The water and GO interactions were calculated by Lennard Jones 6-12 potential between the oxygen and carbon atom using $\epsilon = 0.0937$ kcal/mol and $\sigma = 3.19$ Å [32]. All coulombic forces were calculated using a particle-particle particle-mesh (PPPM) solver. The simulations were performed under the NVT canonical ensemble at 300 K. Temperature control was managed using the Nose-Hoover thermostat. The system energy was first minimised using the conjugate gradient (CG) algorithm and was then run at a timestep of 0.5 femtoseconds.

REFERENCES

[1] T. Kuilla, S. Bhadra, D. Yao, N. H. Kim, S. Bose, and J. H. Lee, "Recent advances in graphene based polymer composites," *Progress in Polymer Science*, vol. 35, no. 11, pp. 1350 – 1375, 2010.

[2] G. Eda and M. Chhowalla, "Chemically derived graphene oxide: Towards large-area thin-film electronics and optoelectronics," *Advanced Materials*, vol. 22, no. 22, pp. 2392–2415, 2010.

[3] S. H. Aboutalebi, R. Jalili, D. Esrafilzadeh, M. Salari, Z. Gholamvand, S. Aminorroaya Yamini, K. Konstantinov, R. L. Shepherd, J. Chen, S. E. Moulton, P. C. Innis, A. I. Minett, J. M. Razal, and G. G. Wallace, "High-performance multifunctional graphene yarns: Toward wearable all-carbon energy storage textiles," *ACS Nano*, vol. 8, no. 3, pp. 2456–2466, 2014.

[4] F. Yavari and N. Koratkar, "Graphene-based chemical sensors," *The Journal of Physical Chemistry Letters*, vol. 3, no. 13, pp. 1746–1753, 2012.

[5] B. Kim, W. Cho, W. Lee, S. Kim, R. Jalili, S. Park, G. Wallace, K. Yu, and S.-J. Chang, "Capacitive behaviour of thermally reduced graphene oxide in a novel ionic liquid containing di-cationic charge," *Synthetic Metals*, vol. 193, no. 0, pp. 110 – 116, 2014.

[6] R. Jalili, S. H. Aboutalebi, D. Esrafilzadeh, R. L. Shepherd, J. Chen, S. Aminorroaya-Yamini, K. Konstantinov, A. I. Minett, J. M. Razal, and G. G. Wallace, "Scalable one-step wet-spinning of graphene fibers and yarns from liquid crystalline dispersions of graphene oxide: Towards multifunctional textiles," *Advanced Functional Materials*, vol. 23, no. 43, pp. 5345–5354, 2013.

[7] M. Cai, D. Thorpe, D. H. Adamson, and H. C. Schniepp, "Methods of graphite exfoliation," *J. Mater. Chem.*, vol. 22, pp. 24992–25002, 2012.

[8] A. M. Dimiev and J. M. Tour, "Mechanism of graphene oxide formation," *ACS Nano*, vol. 8, no. 3, pp. 3060–3068, 2014.

[9] R. Jalili, S. H. Aboutalebi, D. Esrafilzadeh, K. Konstantinov, S. E. Moulton, J. M. Razal, and G. G. Wallace, "Organic Solvent-Based Graphene Oxide Liquid Crystals: A Facile Route toward the Next Generation of Self-Assembled Layer-by-Layer Multifunctional 3D Architectures," *ACS Nano*, vol. 7, no. 5, pp. 3981–3990, 2013.

[10] D. R. Dreyer, S. Park, C. W. Bielawski, and R. S. Ruoff, "The chemistry of graphene oxide," *Chemical Society Reviews*, vol. 39, no. 1, pp. 228–240, 2010.

[11] R. Jalili, S. H. Aboutalebi, D. Esrafilzadeh, K. Konstantinov, J. M. Razal, S. E. Moulton, and G. G. Wallace, "Formation and processability of liquid crystalline dispersions of graphene oxide," *Mater. Horiz.*, vol. 1, pp. 87–91, 2014.

[12] Y. Zhu, S. Murali, W. Cai, X. Li, J. W. Suk, J. R. Potts, and R. S. Ruoff, "Graphene and graphene oxide: Synthesis, properties, and applications," *Advanced Materials*, vol. 22, no. 35, pp. 3906–3924, 2010.

[13] S. Naficy, R. Jalili, S. H. Aboutalebi, R. A. Gorkin III, K. Konstantinov, P. C. Innis, G. M. Spinks, P. Poulin, and G. G. Wallace, "Graphene oxide dispersions: tuning rheology to enable fabrication," *Mater. Horiz.*, vol. 1, pp. 326–331, 2014.

[14] S. Makharza, G. Cirillo, A. Bachmatiuk, I. Ibrahim, N. Ioannides, B. Trzebicka, S. Hampel, and M. Rümmeli, "Graphene oxide-based drug delivery vehicles: functionalization, characterization, and cytotoxicity evaluation," *Journal of Nanoparticle Research*, vol. 15, no. 12, pp. 1–26.

[15] K. A. Mkhoyan, A. W. Contryman, J. Silcox, D. A. Stewart, G. Eda, C. Mattevi, S. Miller, and M. Chhowalla, "Atomic and Electronic Structure of Graphene-Oxide," *Nano Letters*, vol. 9, no. 3, pp. 1058–1063, 2009.

[16] H. He, T. Riedl, A. Lerf, and J. Klinowski, "Solid-State NMR Studies of the Structure of Graphite Oxide," *The Journal of Physical Chemistry*, vol. 100, no. 51, pp. 19954–19958, 1996.

[17] A. Lerf, H. He, M. Forster, and J. Klinowski, "Structure of Graphite Oxide Revisited," *The Journal of Physical Chemistry B*, vol. 102, no. 23, pp. 4477–4482, 1998.

[18] J. Kim, L. J. Cote, F. Kim, W. Yuan, K. R. Shull, and J. Huang, "Graphene Oxide Sheets at Interfaces," *Journal of the American Chemical Society*, vol. 132, no. 23, pp. 8180–8186, 2010.

[19] W. Cai, R. D. Piner, F. J. Stadermann, S. Park, M. A. Shaibat, Y. Ishii, D. Yang, A. Velamakanni, S. J. An, M. Stoller, J. An, D. Chen, and R. S. Ruoff, "Synthesis and Solid-State NMR Structural Characterization of 13C-Labeled Graphite Oxide," *Science*, vol. 321, no. 5897, pp. 1815–1817, 2008.

[20] B. J. Cox, N. Thamwattana, and J. M. Hill, *Mechanics of atoms and fullerenes in single-walled carbon nanotubes. I. Acceptance and suction energies*, vol. 463. 2007.

[21] J.-A. Yan and M. Y. Chou, "Oxidation functional groups on graphene: Structural and electronic properties," *Physical Review B*, vol. 82, no. 12, p. 125403, 2010. PRB.

[22] A. K. Rappe, C. J. Casewit, K. S. Colwell, W. A. Goddard, and W. M. Skiff, "UFF, a full periodic table force field for molecular mechanics and molecular dynamics simulations," *Journal of the American Chemical Society*, vol. 114, no. 25, pp. 10024–10035, 1992.

[23] D. Stauffer, N. Dragneva, W. B. Floriano, R. C. Mawhinney, G. Fanchini, S. French, and O. Rubel, "An atomic charge model for graphene oxide for exploring its bioadhesive properties in explicit water," *The Journal of Chemical Physics*, vol. 141, no. 4, p. 044705, 2014.

[24] R. J. W. E. Lahaye, H. K. Jeong, C. Y. Park, and Y. H. Lee, "Density functional theory study of graphite oxide for different oxidation levels," *Physical Review B*, vol. 79, no. 12, p. 125435, 2009. PRB.

[25] S. Pei and H.-M. Cheng, "The reduction of graphene oxide," *Carbon*, vol. 50, no. 9, pp. 3210–3228, 2012.

[26] A. Martín-Rodríguez, J. de D. López-González, and F. Domínguez-Vega, "Products of oxidation at 0°C of mineralogical and artificial graphite - II. Density and interlaminar surface area," *Carbon*, vol. 7, no. 5, pp. 589–594, 1969.

[27] A. Lerf, A. Buchsteiner, J. Pieper, S. Schöttl, I. Dekany, T. Szabo, and H. P. Boehm, "Hydration behavior and dynamics of water molecules in graphite oxide," *Journal of Physics and Chemistry of Solids*, vol. 67, no. 5-6, pp. 1106–1110, 2006.

[28] W. Humphrey, A. Dalke, and K. Schulten, "VMD – Visual Molecular Dynamics," *Journal of Molecular Graphics*, vol. 14, pp. 33–38, 1996.

[29] D. A. Dikin, S. Stankovich, E. J. Zimney, R. D. Piner, G. H. B. Dommett, G. Evmenenko, S. T. Nguyen, and R. S. Ruoff, "Preparation and characterization of graphene oxide paper," *Nature*, vol. 448, no. 7152, pp. 457–460, 2007.

[30] N. V. Medhekar, A. Ramasubramaniam, R. S. Ruoff, and V. B. Shenoy, "Hydrogen Bond Networks in Graphene Oxide Composite Paper: Structure and Mechanical Properties," *ACS Nano*, vol. 4, no. 4, pp. 2300–2306, 2010.

[31] A. Buchsteiner, A. Lerf, and J. Pieper, "Water Dynamics in Graphite Oxide Investigated with Neutron Scattering," *The Journal of Physical Chemistry B*, vol. 110, no. 45, pp. 22328–22338, 2006.

[32] N. Wei, C. Lv, and Z. Xu, "Wetting of Graphene Oxide: A Molecular Dynamics Study," *Langmuir*, vol. 30, no. 12, pp. 3572–3578, 2014.

[33] B. Rezania, N. Severin, A. V. Talyzin, and J. P. Rabe, "Hydration of Bilayered Graphene Oxide," *Nano Letters*, vol. 14, no. 7, pp. 3993–3998, 2014.

[34] Y. Huang, X. Zhang, Z. Ma, W. Li, Y. Zhou, J. Zhou, W. Zheng, and C. Q. Sun, "Size, separation, structural order, and mass density of molecules packing in water and ice," *Sci. Rep.*, vol. 3, 2013.

[35] A. C. T. van Duin, S. Dasgupta, F. Lorant, and W. A. Goddard, "ReaxFF: A Reactive Force Field for Hydrocarbons," *The Journal of Physical Chemistry A*, vol. 105, no. 41, pp. 9396–9409, 2001.